

Study of Heat Transfer on Cemented Hip Replacement

Abstract-This work involved the study of heat transfer in a cemented hip replacement. The recent rise in cemented hip replacement in Orthopaedic and trauma surgery is of alarming concern to the material usage and conditions it's been subjected to. Bone cementing which is the main technology providing the bonding mechanism between the femur cavity and the prosthesis stem is the polymerization reaction between, the powder and liquid monomer which is an exothermic reaction. This is of concern to biomechanics engineers on the heat transfer mechanisms between the bone cement, the prosthesis stem and the femur bone. The ANSYS 15.0 software was used in conjunction with the Autodesk software to model the scenario and simulate it using steady state thermal-structural analysis. It was found that the temperature that resulted from the exothermic reaction of the PMMA polymer (used as bone cement) raised the temperature in the assembly creating a heat flux amounting to $5.11 \times 10^{-7} \text{ W/m}^2$ in which only $2.83 \times 10^{-7} \text{ W/m}^2$ got to the femur bone as other has been absorbed by the prosthesis stem and the femur bone. The specific heat capacities of PMMA and femur bone were calculated as 1.297 kJ/kg.K and 0.59 kJ/kg.K respectively. The Young Modulus for PMMA was found as 28.78 GPa and 18.79 GPa for femur bone. These show that it is possible to determine these properties from the simulation studies.

Keywords- Heat Transfer, Femur bone, Prosthesis stem, Thermal-structural analysis, Specific heat capacity, Bone cementing

1. Introduction

Bone cementing over the years has been very successfully used in providing aid for artificial joints such as hip joints, knee joints, shoulder and elbow joints for more than half a century. This technology which is newly introduced in Nigeria has indigenous companies trying to work out the suitable local materials that can be engaged in bone cementing that is comparable to the imported counterpart (McLaren, 2004). Artificial joints like the hip joints are usually anchored by bone cementing which is meant to fill the free space that would exist between the prosthesis and the bone. Hence it plays a vital role in creating an elastic limit or zone due to thermal loads agitated by external effects such as walking, running, sitting and even body weights (Kweon et al, 2011). This is essential because the human hip is acted on by approximately 10-12 times the body weight and therefore the bone cement must be able to contain the forces acting on the hips by absorbing the forces and pressures at the contact segment to ensure that the artificial implant remains in place over the long term (Vaishya et al, 2013). Bone cement chemically is nothing more than Plexiglas (polymethylmethacrylate "PMMA"). PMMA was clinically used the first time in 1940 in plastic surgery to fill up the gaps in the skull. Comprehensive clinical tests of the compatibility of bone cements with the body were conducted before their use in surgery. The excellent tissue compatibility of PMMA allowed it to be used as bone cement for anchorage of head prostheses in the 1950s (Vaishya et al, 2013).

Charnley after experimenting with various materials while working at Manchester University, eventually settled on PMMA -a viscous dough which he formed by mixing the powder with the liquid monomer (Gonçalves et al, 2012). In 1958, he performed his first case in Manchester. Charnley was the first to apprehend that PMMA could be easily used to fill the medullar canal and merge with the bone morphology. The cement acted to increase the biomechanical stability and decrease the stress on the implant and he settled on the idea of using cement as a 'grout' for the hip implants (Gonçalves et al, 2012). Despite all the early scepticism, PMMA is being used as bone cement for implant fixation in various Orthopaedic and trauma surgeries to this day.

48 In the usage of bone cementing, there exist some external problematic factors that lead to
 49 adverse effects of bone cementing. With different loadings acting on the joint such as body
 50 weight, walking and running, the internal friction increases thereby increasing the internal
 51 temperature of the cemented bone. This leads to an obstruct expansion of the cemented bone
 52 above the elastic zone and hence causes aseptic loosening (Mjoberg, et al, 1984).

53 Additionally, this problem is based on incomplete heat transfer in the bone-cement-prosthesis
 54 system. It is also believed that mechanical properties of the cement and thermal and chemical
 55 injuries of the bone tissue in the bone-cement interface are two main factors that affect the
 56 heat transfer process in the system (Akanksha et al, 2014).

57 Even though the practices and obtainability of various types of bone cement have greatly
 58 progressed over the past century, further research still continues to develop its more clinical
 59 applications and to reduce the adverse effects associated with their usage. The aim of this
 60 research is to study the heat transfer on a cemented hip replacement joint.

61 2. Theoretical Concepts

62 The Governing Equations

63 The heat-flux equation is the energy balance for heat conduction through an infinitesimal
 64 non-moving volume. The energy balance equation applied to a system of finite volume
 65 according to Cengel and Ghajar, (2015):

$$66 \quad \left. \frac{dH}{dt} \right|_p = \dot{Q} \rightarrow \int_V \rho c \frac{\partial T}{\partial t} dV = - \int_A \vec{q} \cdot \vec{n} dA + \int_V \phi dV \quad (1)$$

67 Where; \dot{Q} is some energy release per unit volume (by chemical reactions), sometimes written
 68 as \dot{q}_{gen} . Eq.(1) can be read as "the time-increment of enthalpy within the volume due to the
 69 heat input through the frontier plus the energy dissipation in the interior"; the minus sign
 70 coming from the choice of \vec{n} as the normal outwards vector. When the Gauss-Ostrogradski
 71 theorem of vector calculus is used to transform the area-integral to the volume-integral, and
 72 Eq.(1) becomes according to Cengel and Ghajar, (2015):

$$73 \quad \int_V \rho c \frac{\partial T}{\partial t} dV = - \int_A \vec{q} \cdot \vec{n} dA + \int_V \phi dV = - \int_V \nabla \cdot \vec{q} dV + \int_V \phi dV \rightarrow$$

$$74 \quad \xrightarrow{V \rightarrow 0} \rho c \frac{\partial T}{\partial t} = - \nabla \cdot \vec{q} + \phi \quad (2)$$

75 To solve this numerically by the finite element method, we multiply Eq.(2) by a weighting
 76 function $v(x)$, and then set the total weighted residual error to zero (Tang, 2011)

$$77 \quad \int_{\Omega} v p C_p \frac{\partial T}{\partial t} d\Omega - \int_{\Omega} v \nabla \cdot (k \nabla T) dv = 0$$

78 (3)

79 Using the symmetry of $\nabla \cdot (vk \nabla T)$, we have

$$80 \quad v \nabla \cdot (k \nabla T) = \nabla \cdot (vk \nabla T) - k \nabla T \cdot \nabla v.$$

81 (4)

82 Substituting Eq.(3) into Eq.(4) and using the divergence theorem;

$$83 \quad \int_{\Omega} v p C_p \frac{\partial T}{\partial t} d\Omega + \int_{\Omega} k \nabla T \cdot \nabla v d\Omega = \int_{\partial\Omega} vk \frac{\partial T}{\partial n} ds. \quad (5)$$

84 Imposing the boundary conditions into Eq.(5) yields;

$$85 \quad \int_{\Omega} v p C_p \frac{\partial T}{\partial t} d\Omega + \int_{\Omega} k \nabla T \cdot \nabla v d\Omega + \int_{\partial\Omega} v h_{\infty} T ds. = \int_{\partial\Omega} v h_{\infty} T_{ext} ds.$$

86 (6)

87 Therefore, the variation statement for the boundary value problem can be stated as follows
 88 according to (Tang, 2011):

89 Find $T = T(x, t) \in H^1(\Omega)$ such that for every $t \in I$

90
$$(T_t, v) + a(T, v) = L(v) \quad \forall v \in H_0^1(\Omega)$$

91 (7)

92 Where; $(T_t, v) + a(T, v) = L(v) \quad \forall v \in H_0^1(\Omega)$

93
$$T(x, 0) = \hat{T}(x)$$

94
$$(T, v) = \int_{\Omega} v p C_p \frac{\partial T}{\partial t} d\Omega.$$

95 Let $H^1_h(\Omega)$ be a finite dimensional subspace of H^1 with basic functions $\{\phi_1, \phi_2, \dots, \phi_n\}$.

96 Then, the variation problem is approximated by:

97 Find $Th(x, t) \in H^1_h$ such that $Th(x, 0) = \hat{T}(x)$ and $\left(\frac{\partial Th}{\partial t}, v_h\right) + a(Th, v_h) = L(v_h), \forall v_h \in H^1_h.$

98 (8)

99 In the usual way, we introduce a discretization of Ω as a union of elements Ω_e , i.e.,

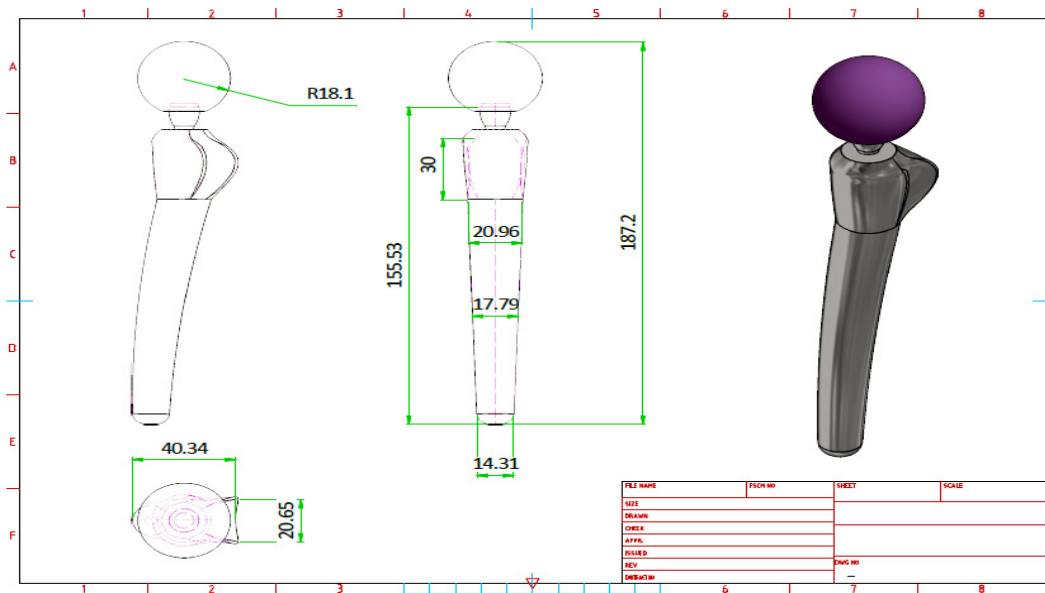
100 $\Omega \rightarrow \cup_{e \in \mathcal{E}} \Omega_e$ and approximate $T(x, t)$ at t by:

101
$$T = \sum_{j=1}^N \phi_j T_j, \quad v = \sum_{j=1}^N \phi_j v_j$$

102 (9)

103 **Femur Design:** For the prosthesis stem which is inserted into the femur bone, it is essential
 104 to dimensionally design each component of the hip replacement for determining the heat
 105 transfer characteristics. The prosthesis stem spans 155.5mm long, with a ball of 36mm in
 106 diameter. The stem exhibits 3 diametric segments. The top most stem is 20.96mm, the second
 107 segment is 17.79mm and the bottom segment of the stem is 14.31mm, see fig. 1. This is
 108 because of the non-uniformity of the femur hip and for the easy of insertion and removal of
 109 the prosthesis stem.

110

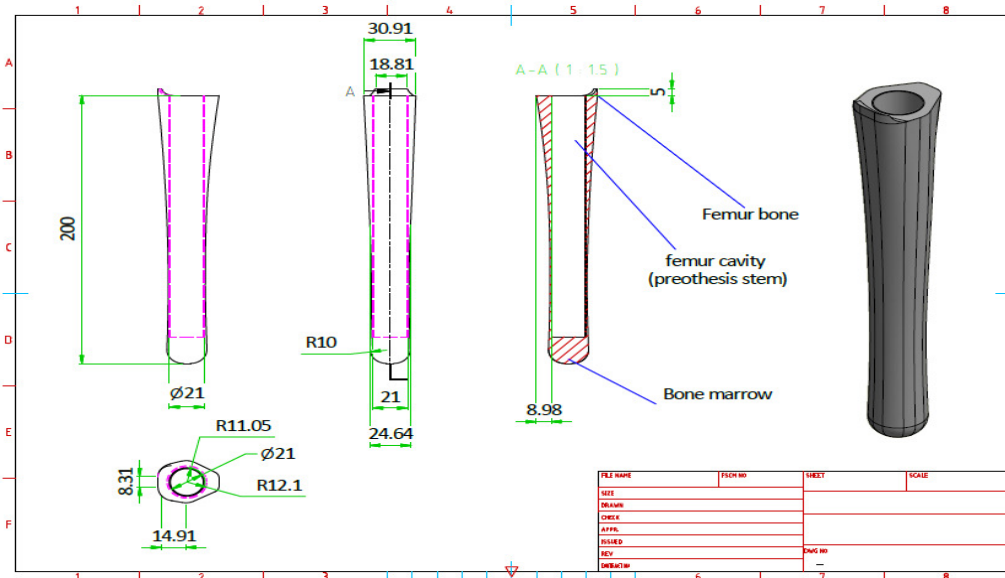


111

112

113 **Figure 1: Isometric and Orthographic drawing of the prosthesis stem**

114 The femur design was accomplished using the Autodesk Inventor software. The top section
 115 bone was designed with a diameter of 30.91mm while the bottom section was 21mm in
 116 diameter; a cavity bored using the cut extrude function was made having a diametric hole of
 117 the top section of 18.81mm while the bottom section of the cavity was 20mm. The gap
 118 between the femur and the cavity gives the allowance for the bone cementing operation, see
 119 fig. 2. The bone spans a length of about 200mm which was considered from the design
 120 standard.
 121



122
 123 **Figure 2: Isometric and orthographic drawing of the femur bone**

124 **2. Experimentation**

125 **Materials and Material Properties:** PMMA used in this study as the bone cement as two
 126 main components: the powder and the liquid. The densities of both components have been
 127 reported in the literature (Berbmann et al, 2001) as about 1100kg/m^3 but in order to simplify
 128 the model, the material properties of the final PMMA mixture are considered. The mass
 129 density of the bone cement mixture is assumed to be constant $1.1 \times 10^{-6} \text{ kg/mm}^3$ as proposed
 130 by Baliga et al, (1992). According to Perez et al., (2009), the specific heat of bone cement c
 131 is reported to be either temperature dependent $c = 1.25 \times 10^3 + 6.5T/\text{kg}^\circ\text{C}$ or constant varying
 132 between 1450 and $2000\text{J/kg}^\circ\text{C}$. The thermal conductivity value, k Cement, is assumed to be
 133 constant, $0.0002\text{W/mm}^\circ\text{C}$. (Perez et al, 2009). Bone cement material properties change
 134 depending on the polymerization process involved and the modulus of elasticity E which is
 135 time- dependent. Experimental studies (Lewis, 1997; Perez et al, 2009) on the modulus of
 136 elasticity of the fully solidified cement have reported a wide range of values: 1583–4120MPa.
 137 In the present model, an average value of 2400MPa was assumed. The first important new
 138 assumption in the numerical model proposed here is the consideration of the modulus of
 139 elasticity (E) of the PMMA mixture as a function of the modulus of elasticity of the fully
 140 solidified cement (E solidified) and its polymerization fraction p .

141 The prosthesis stem however, is materialized based on the Metal on Metal (MOM) formation.
 142 Both the socket and the ball are made of either stainless steel, titanium, chromium, cobalt or
 143 some combination of these. For this study, titanium is used.

144

145

Table 1: Physical Properties of PMMA (Wapler et al, 2014)

Physical Properties	Value
Density	1.15 - 1.19 g/cm ³
Linear Mould Shrinkage	0.003 - 0.0065 cm/cm
Melt Flow	0.9 – 27 g/10 min

146 PMMA has high mechanical strength, high Young's Modulus and low elongation. It does not
 147 shatter on rupture. It is one of the hardest thermoplastics and is also highly scratch resistant. It
 148 exhibits low moisture and water absorbing capacity, due to which products made have good
 149 dimensional stability. Both of these characteristics increase as the temperature rises. Tables 1
 150 and 2 show some of mechanical and thermal characteristics of PMMA.

151

Table 2: Mechanical and Thermal Properties of PMMA (Wapler et al, 2014)

(a) Mechanical Properties of PMMA		(b) Thermal Properties of PMMA	
Mechanical Properties	Value	Thermal Properties	Value
Hardness, Rockwell M	63 – 97	Specific Heat Capacity	1.46 - 1.47 J/g.°C
Tensile Strength, Ultimate	47 - 79 MPa	Thermal Conductivity	0.19 - 0.24 W/m.K
Elongation at Break	1 - 30 %	Maximum Service Temperature, Air	41 -103 °C
Tensile Modulus	2.2 - 3.8 GPa	Melting Point	130°C

152

153 The thermal stability of standard PMMA is only 65°C. Its resistance to temperature changes
 154 is very good.

155 Titanium is a chemical element with symbol Ti and atomic number 22. It is a lustrous
 156 transition metal with a silver colour, low density, and high strength (table 3). Titanium is
 157 resistant to corrosion in sea water, aqua regia, and chlorine. The two most useful properties of
 158 the metal are corrosion resistance and strength-to-density ratio, the highest of any metallic
 159 element. In its unalloyed condition, Titanium is as strong as some steels, but less dense.

160

Table 3: Properties of Titanium and Human Femur bone (Pal, 2014)

(a) Properties of Titanium		(b) Properties of Human	
Properties	Value	Properties	Thighbone (Femur)
Thermal Expansion	8.6 $\mu\text{m}/(\text{m}\cdot\text{K})$ (25 °C)	Density, g/cm ³	1.6 – 1.7
Thermal Conductivity	21.9 W/(m·K)	Young's Modulus, GPa	10 – 15
Young's Modulus	116 GPa	Tensile Strength, MPa	90 – 130
Shear Modulus	44 GPa	Compressive Stress, MPa	130 – 200
Bulk Modulus	110 GPa	Fracture Strain, %	1 – 3
Poisson Ratio	0.32	Toughness, MPa.m ^{1/2}	1 – 2
		Hardness (Vickers)	50 – 100

161 Bone naturally is brittle in nature. The strength of natural bone varies considerably by type,
 162 composition and age. The compressive strength of the strong outer (cortical) bone of a
 163 thighbone (femur) is typically about 150 MPa, while the spongier inner bone can exhibit a
 164 compressive strength below 10 MPa. In Table 3, typical mechanical property values of an
 165 entire human thighbone are given. For the bone, the following properties of density, Young's
 166 Modulus and Poisson's Ratio are used as 2000 Kg/m³, 2.130 GPa and 0.3 respectively for
 167 analysis. (Pal, 2014)

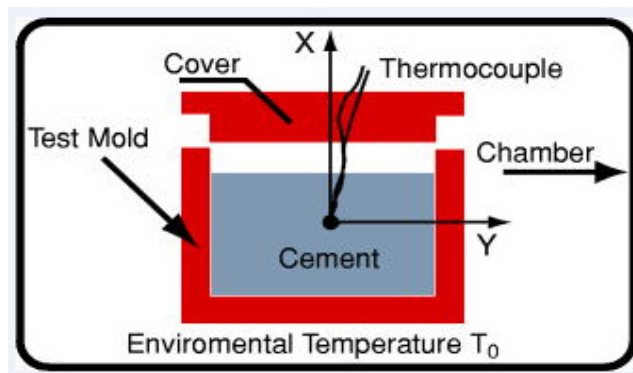
168 The thermal conductivity varies also depending on the dryness nature of the bone. The wet
 169 bone has about four times the thermal conductivity of the dry done. The conductivity is found
 170 to be 0.58±0.018 W/m.K in the longitudinal direction, 0.53±0.030 W/m.K in the
 171 circumferential direction, and 0.54±0.020 W/m.K in the radial direction. Because the

172 directional differences are small, it is concluded that bovine cortical bone can be treated as
 173 thermally isotropic. (Pal, 2014)

174 **Experiment:** The only experiment done was in the mixing of the cement to determine the
 175 appropriate temperature for the simulation studies. PMMA bone cement preparation involves
 176 mixing the solid component, powder, with the liquid component. The ratio is usually 2g of
 177 powder to 1ml of liquid; however, this composition can vary depending on the type of cement
 178 used. Usually the solid part is the polymer, PMMA, plus the initiator, benzoyl peroxide, and
 179 the liquid part is the pure monomer, Methyl methacrylate (MMA), plus the activator. During
 180 the polymerization process, monomer MMA is converted into PMMA, which involves an
 181 exothermic reaction. Mixing together the powder and the liquid components marks the start
 182 of the polymerization process. During the reaction, the cement viscosity increases, slowly at
 183 first, then later more rapidly. Studies have shown that high viscosity cements result in better
 184 prosthetic fixation, as compared to low viscosity cements. Immediately after mixing, a
 185 thermocouple was placed on the bone cement to determine the temperature.

186 The set up used for this purpose is shown in fig.3. The mixing of the bone cement performed
 187 in the ambient temperature of 25°C was repeated seven times within the temperature range
 188 43°C to 47°C at time frame of 160s. The values of maximum temperature and time for each
 189 experiment were recorded on the table 3. This temperature range is within the range of values
 190 reported in literature. Swenson et al, (1981) recorded that the maximum temperature attained
 191 during polymerisation ranged from 60°C to 70°C. Homsy et al, (1972) reported a peak
 192 temperature of 60°C and 70°C of the bone cement. Noble, (1983) reported that the maximum
 193 temperature attained during polymerization ranged from 60°C to 70°C for seven cements
 194 tested.

195



196

197 **Figure 3: Experimental Set-up**

198

Table 4: Values of the recorded temperature

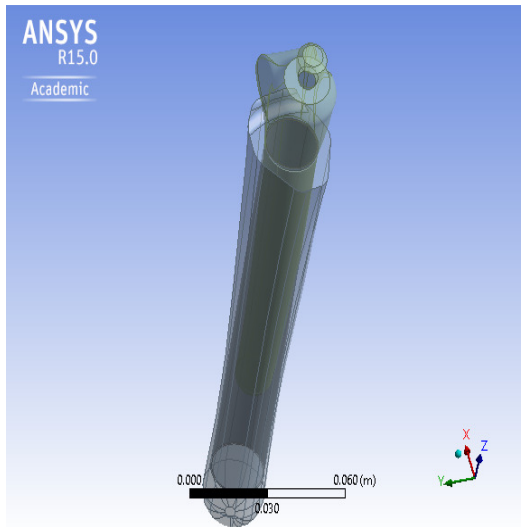
Experimental No.	Maximum Temperature (°C)	Time (s)
1	45	105
2	47	160
3	44.4	100
4	46.5	158
5	47	155
6	46.7	159
7	47	157

199 Since physical experiment using human femur was not performed, the results of the
 200 temperature values in table 4 were used for simulation studies only.

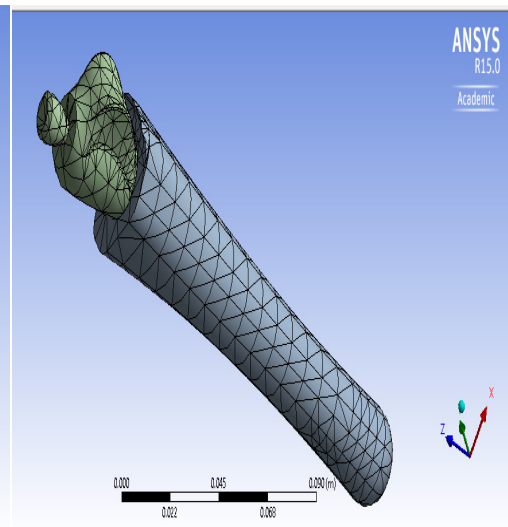
201 **4. Results and Discussion**

202 **Model Analysis:** At this phase, the finite element analysis (FEA) was performed on the
 203 femur bone to simulate the thermal behaviour as the bone cement was visualized placed
 204 alongside the prosthesis stem of the femur cavity. The Ansys software was deployed
 205 alongside with the Autodesk Inventor through a computer aided Engineering to efficiently
 206 and effectively simulate the whole process. After the importation of the assembled model, the
 207 physical and mechanical properties of the materials, PMMA, Titanium, prosthesis stem and
 208 the bone structure, as defined in tables 1 to 3 were used.

209 **Model Preparation:** The geometry was modelled using the Ansys software. The co-ordinates
 210 were set to locate the axis and origin of the geometry. Since the geometry consists of no
 211 movable parts, the contacts areas were set as fixed (fig.4).



212
213 **Figure 4: Assembled geometry**
214 **for Mesh preparation**



215
Figure 5: Meshing of the
assembled Model

216 After this, the model was discretized into finite elements. The discretization reduced the
 217 model into smaller elements with nodes. For a discreet setting, the meshing process took the
 218 tetrahedral elemental structure. This element accommodated the processing of 3D models in
 219 which the x, y and z axes were considered in the setting of the boundary conditions and the
 220 acknowledgment of their effects. Fig.5 is the meshed geometry showing the nodes and
 221 elements of the assembled bone. The total elements and nodes recorded were 20545 and
 222 127247 respectively (table 5).

223

Table 5: Mesh Configurations

Object Name	<i>Mesh</i>
State	Solved
Defaults	
Physics Preference	Mechanical
Relevance	0
Sizing	
Use Advanced Size Function	Off
Relevance Center	Coarse
Element Size	Default

Initial Size Seed	Active Assembly
Smoothing	Medium
Transition	Fast
Span Angle Center	Coarse
Minimum Edge Length	1.5556e-004 m
Inflation	
Use Automatic Inflation	None
Inflation Option	Smooth Transition
Transition Ratio	0.272
Maximum Layers	5
Growth Rate	1.2
Inflation Algorithm	Pre
View Advanced Options	No
Statistics	
Nodes	127247
Elements	20545
Mesh Metric	None

224 A finite element model of the bone cemented joint was produced using the Computer Aided
 225 Engineering (CAE) package, ANSYSv15.0. The precision and accuracy of the model
 226 depends upon its element size or number of nodes and time step size. The increase in number
 227 of nodes not only increases the accuracy of the model, but also increases the processing time
 228 of the model. An optimum solution could be reached by increasing node density near the
 229 region of high temperature gradient, which is in the vicinity of weld line, and decreasing node
 230 density near the region of low temperature gradient, which is away from the weld line

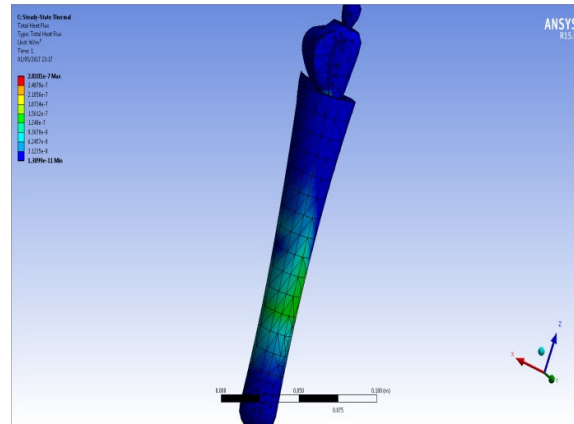
231 **Boundary conditions:** The boundary conditions were set with the three different materials
 232 assembled. The one basic input is the temperature at which the Bone cement gets to the
 233 termination stage of the polymer process; it is therefore imperative that we determine the
 234 effect of that input. The conductive and convective factors are put in place from the
 235 prosthesis stem and bone cement respectively.

236 The outputs needed are the heat flux and the structural effects occurring around the assembly.
 237 Hence, a thermostatic analysis was carried out with ambient temperature of 25°C. Since the
 238 initiation and termination of the polymerization process of the PMMA polymer is between
 239 40°C and 47°C, extreme boundary condition will occur when the initiation process reaches a
 240 peak temperature of 50°C. Here, the heat flux will create several effects thermally and
 241 structurally.

242 **Simulation studies:** The simulation carried out in the present study shows a maximum
 243 temperature of 57°C at the bone cement. Maletijt et al, (1987) and Yamamoto et al, (1998)
 244 have been clinically testing bioactive bone cement which consists of CaO-SiO₂-P₂O₅-MgO-
 245 CaF₂ and that gives maximum temperature of 60°C during polymerisation. The highest
 246 surface temperature for PMMA cement composite was 60°C, while that for bioactive bone
 247 cement was 35°C. McLaren, (2004), found the highest temperature to range from 41.4°C to
 248 43.1°C. Peter et al., (1999) investigated biodegradable bone cement which consisted of
 249 PPF(polypropylenefumarate). Its maximum cross-linking temperature was between 38°C and
 250 48°C, which was much lower than the cross-linking temperature of 94°C for PMMA cement

251 (Peter et al, 1999). Based on these comparisons, experimental values of temperature obtained
 252 in this work can be seen to be within ranges of other temperatures recorded in literature.

253 With the ambient temperature taken at 25°C for all simulations using Ansys software, the
 254 total surface area was found to be $2.95 \times 10^{-6} \text{m}^2$.



255

Figure 6: 40 degrees PMMA Thermal effect

256

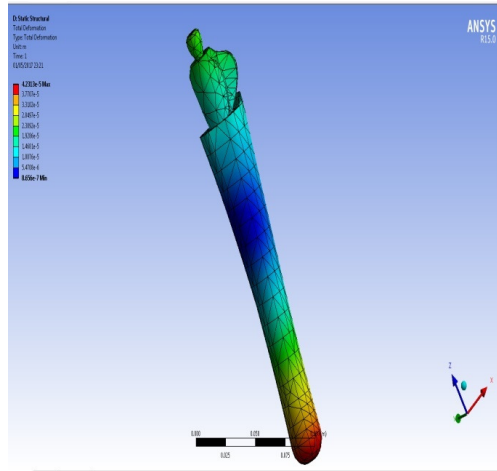
257 From the coding of the simulation effect (fig. 6), it is observed that femur bone received a
 258 heat flux of about $1.249 \times 10^{-7} \text{W/m}^2$ which emanated from the PMMA bone cement and the
 259 heat flux reaching the prosthesis stem was $2.810 \times 10^{-7} \text{W/m}^2$. Although the heat flux may do
 260 little or nothing to the femur or prosthesis stem, it should be noted that the heat is also
 261 transferred to the blood vessels which might have some effects generally.

262 Thermal-structural analysis was carried out. The equivalent Von Mises stress, the total
 263 deformation, equivalent Von Mises strain and strain energy were determined parametrically
 264 within the ranges of loads from the boundary conditions. At 40°C, the structural effects were
 265 observed.

266 In fig.(7), the deformation experienced was found to be very small. At the bottom of the
 267 assembly, the value was about $4.29 \times 10^{-5} \text{m}$. The ends of the assembly experienced the most
 268 deformational effect. The centre received the least deformation effect of about $8.65 \times 10^{-7} \text{m}$
 269 (fig. 7).

270 From fig.(8): In terms of the equivalent stress, the femur bone received lower stress of about
 271 2.573MPa from the lower to the upper part of the femur bone while the bone cement and the
 272 prosthesis stem received a maximum of 12.39MPa. These stresses are far below the yield
 273 strength or ultimate strength of the femur or prosthesis stem but still have some impact on the
 274 general assembly (fig. 8).

275



276

277 **Figure 7: Total deformation of the**
278 **Thermo-structural analysis effect**

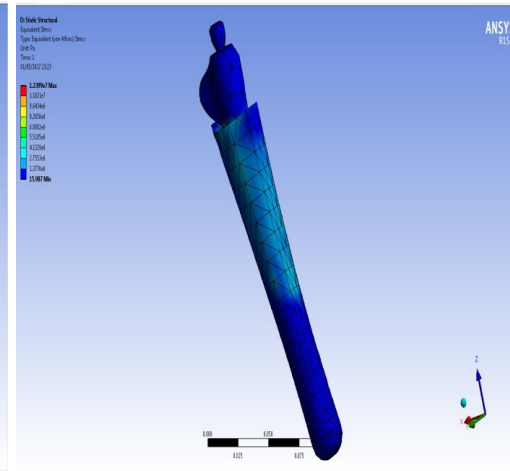
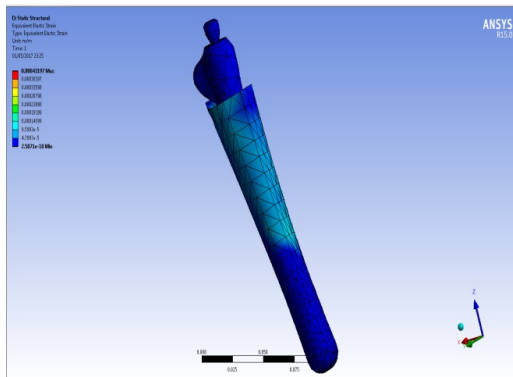


Figure 8: Equivalent stress of the
thermo-structural analysis effect



279

280 **Figure 9: Equivalent strain of the**
281 **Thermo-structural analysis effect**

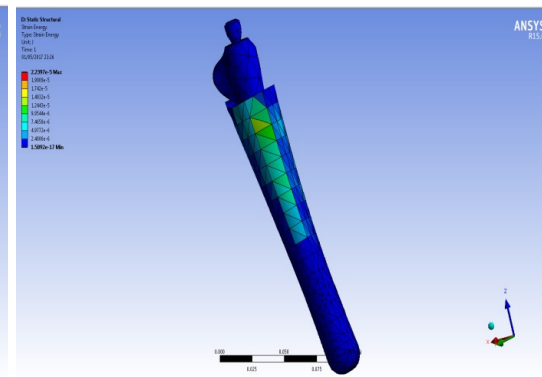


Figure 10: Strain Energy of the
Thermo-structural analysis effect

282
283
284
285

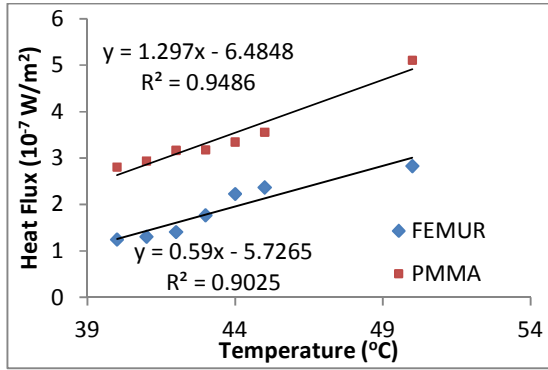
The strain (fig. 9) which is the ratio of the elongation to the original length in the x, y and Z coordinates showed a strain of 0.000143m at the femur bone and about 0.000431m at the bone cement. This is also the case in the strain energy as well (fig. 10). All the results of the simulation studies are summarized in figs. 11 to 13.

286
287
288
289
290

The heat flux can be seen in both cases to increase with an increasing temperature. It ranged from $1.25 \times 10^{-07} \text{ W/m}^2$ at 40°C to $2.83 \times 10^{-07} \text{ W/m}^2$ at 50°C for the femur bone, and from $2.81 \times 10^{-07} \text{ W/m}^2$ at 40°C to $5.11 \times 10^{-07} \text{ W/m}^2$ at 50°C for PMMA. The slopes of the graphs (fig. 11) for both the PMMA and the femur bone gave approximately the specific heat capacities of the two materials respectively: $C_p = \frac{dq}{dT}$. These are given for both the PMMA

291
292
293
294
295
296
297
298

and Femur bone as: $C_p = 1.297 \text{ kJ/kg} \cdot ^\circ\text{k}$ and $C_p = 0.59 \text{ kJ/kg} \cdot ^\circ\text{k}$ respectively. According to Landgraf et al, (2015), the specific heat capacity of the PMMA was $1.2 \text{ kJ/kg} \cdot \text{K}$. This differs from the result of this work by about 7.6%. Fukushima et al (2002) recorded the specific heat capacity of the bone cement (PMMA) as $1.6 \text{ kJ/kg} \cdot \text{K}$ which is about 18% different from the value reported in this work. For the femur bone (cortical bone), Fukushima et al, (2002) found the specific heat capacity to be $0.46 \text{ kJ/kg} \cdot \text{K}$ which is about 22% different from the result of this work. These percentage differences may be attributable to minor errors in the simulation studies.



299

300 **Fig.11: Heat flux as a function of temperature**
 301 **bone**

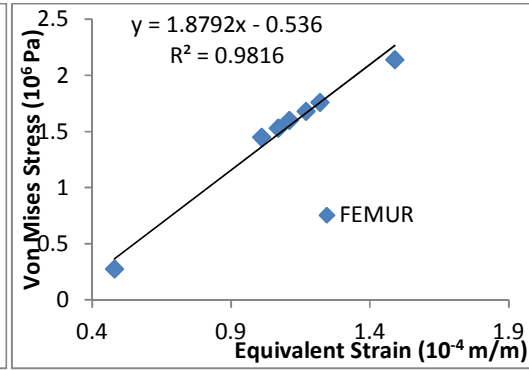
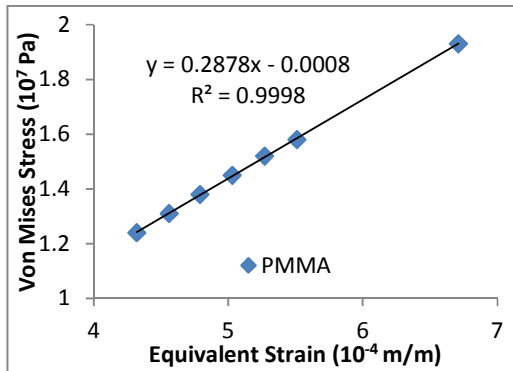


Fig. 12a: Stress-strain relationship: femur



302

303 **Fig. 12b: Stress - strain relationship for PMMA**
 304 **relation**

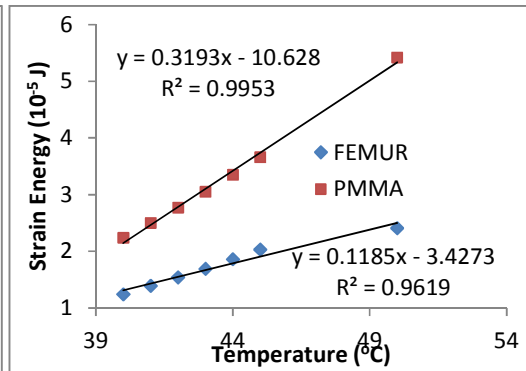


Fig. 13: Strain energy-temperature

305 The data obtained were fitted to polynomial of the form: $C_p = \alpha + \beta T + \gamma T^2 + \lambda T^3$ to give
 306 the temperature dependence of the specific heat capacity of the femur bone as: $C_p = 1 \times 10^{-6} -$
 307 $9 \times 10^{-8} T + 5 \times 10^{-10} T^2 + 4 \times 10^{-12} T^3$ with $R^2 = 0.9774$. For the bone cement the temperature
 308 dependence of the specific heat capacity was found to be: $C_p = 3 \times 10^{-7} + 2 \times 10^{-8} T - 5 \times 10^{-$
 309 $10} T^2 + 4 \times 10^{-12} T^3$ with $R^2 = 0.9926$.

310 The Von Mises stress which is the resultant stress from the three coordinates that describe the
 311 failure criteria of the material in question is seen to increase as the temperature increases for
 312 both the PMMA cement and the femur. It varied from $2.76 \times 10^{+05}$ Pa at 40°C to $2.14 \times 10^{+06}$ Pa
 313 at 50°C for femur and from $1.24 \times 10^{+07}$ Pa at 40°C to $1.93 \times 10^{+06}$ Pa at 50°C for PMMA. The
 314 strain effect which describes the ratio of the deformation to the original length explains the
 315 degree to which a material can be strained beyond its original form. It is seen that the strain
 316 increases as the temperature increases for both the PMMA cement and the femur. The young
 317 modulus for each of PMMA cement and the Femur was determined from the slope of stress-
 318 strain curves of fig. 12 as 28.78 GPa and 18.79 GPa, respectively.

319 The Young Modulus for PMMA of 28.78 GPa, is larger than the range of values reported in
 320 MIT property data base (2017). The differences in the values of Young's Modulus may be
 321 due to the fact that the simulation in this work used different cement properties than those
 322 used at MIT; they considered pure PMMA while this work considered a combined assemble
 323 of the PMMA and the titanium prosthesis stem. The incorporation of titanium of course
 324 would make the prosthesis stronger, and the fact that the result of this work is far larger is
 325 expected.

326 The Young's Modulus for femur bone of 18.79 GPa is comparable with literature values. Rho
327 et al., (1993), using both ultrasonic and micro-tensile measurements found the average
328 trabecular Young's Modulus to be 14.8 ± 1.4 GPa and 10.4 ± 3.5 for bone cement giving an
329 overall average value of 12.6 GPa. This result is smaller than that of this study by about
330 33%. They found the average Young's Modulus of micro-specimens of cortical bone
331 measured ultrasonically and mechanically as 20.7 ± 1.9 GPa and 18.6 ± 3.5 GPa giving an
332 overall average of 19.65 GPa. This is higher than that of this work by about 4%. The result
333 of this work appears to correlate more with that of micro-specimens of cortical bone
334 determined by the ultrasonic and mechanical tests.

335 The strain energy is the energy required to strain a material by causing deformations against
336 its original length. We can observe that the strain energies of both the femur bone and the
337 PMMA bone cement increase significantly with an increase in temperature (fig. 13). The
338 strain energy per degree rise in temperature is 0.3193×10^{-5} J/C for PMMA and 0.1185×10^{-5} J/C for
339 the Femur. This shows that the cement is more sensitive to temperature rise than the bone.

340 5. Conclusion

341 The heat transfer effect in a cemented hip replacement was studied. An experiment was
342 performed to determine the temperature range to be used for simulation. PMMA bone cement
343 preparation involved the mixing of the solid component, powder, with the liquid component
344 in the operating room. That is, the polymer plus the initiator, benzoyl peroxide, and the liquid
345 monomer, Methyl methacrylate (MMA), plus the activator, were mixed. During the
346 polymerization process, monomer MMA was converted into PMMA, which involved an
347 exothermic reaction. The temperature that resulted during this process ranged from 43°C to
348 47°C . Various literatures reported a temperature ranging from 38°C to 70°C , thus a
349 temperature range of 40 to 50 was used for simulation.

350 The bone and bone cement thermal and physical properties were obtained from the literature
351 and used to design the femur using ANSYS software-bone cement combination. This design
352 exercise properly defined the model geometry, setting the contacts as fixed bonds as there
353 were no moving parts. After this the model was discretized into finite elements, reducing the
354 model into smaller elements with nodes. These elements were defined by fundamental
355 equations and boundary conditions. The meshing process took the tetrahedral elemental
356 structure. The total elements and nodes recorded were 20545 and 127247 respectively. A
357 finite element model of the bone cemented joint was produced using the Computer Aided
358 Engineering (CAE) package, ANSYSv15.0. The increased number of nodes increased not
359 only the accuracy of the model, but the processing time of the model.

360 The outputs in the analysis included the heat flux, the deformation, von Mises stress and
361 strain energy as a function of temperature. The simulation gives the total surface area being
362 affected by the increasing temperature as $2.95 \times 10^{-6} \text{m}^2$. From the temperature dependence of
363 the heat flux, the specific heat capacities were found to be $1.297 \text{kJ/kg}^{\circ}\text{K}$ and $0.59 \text{kJ/kg}^{\circ}\text{K}$
364 respectively for PMMA and Femur bone. Other important findings included the young
365 modulus of femur of 18.79 GPa and of PMMA as 28.78 GPa. These are comparable with
366 literature values. Other quantities that are affected by the temperature are the deformations,
367 strain and strain energy. It was seen that the temperature that resulted from the exothermic
368 reaction of the PMMA polymer raised the temperature in the assembly creating a heat flux
369 amounting to $5.11 \times 10^{-7} \text{W/m}^2$ in which only $2.83 \times 10^{-7} \text{W/m}^2$ got to the femur bone as other
370 has been absorbed by the prosthesis stem and the femur bone. Other effects which were
371 structural might have occurred during this process.

372 **References**

- 373 Akanksha B., Arjun C., Cila H. (2014), Heat transfer model for deep tissue injury: a step
374 towards an early thermographic diagnostic capability. *Diagnostic Pathology*, 9: 1 –
375 36.
- 376 Baliga B. R., Rose P. I., Ahmed A. M. (1992), Thermal modelling of polymerizing
377 considering temperature – distribution heat generation, *J Biomech. Eng.*, 114: 251 –
378 259.
- 379 Bergmann G., Graichenn F., Rohlmann A., Verdonschot N. and van Lenthe G. H. (2001),
380 Frictional heating of total hip implants Part 2: finite element study. *Journal of*
381 *Biomechanics*, 34: 429 – 435.
- 382 Cengel Y. A. and Ghajar A. J. (2015), Heat and Mass Transfer: Fundamentals &
383 Applications. *McGraw-Haill Education Pvt Ltd*, 5th Ed.2015: 1 – 879.
- 384 Fukushima H., Hashimoto Y., Yoshiya S., Kurosaka M., Matsuda M., Kawamura S.,
385 Iwatsubo T. (2002), Conduction Analysis of Cement Interface Temperature in Total
386 Knee Arthroplasty. *Kobe J. Med. Sci.*, 48(1 – 2): 63 – 72.
- 387 Goncalves D., Thompson T. J. U., Cunha E. (2012), Implications of heat-induced changes in
388 bone on the interpretation of funerary behaviour and practice. *Journal of*
389 *Archaeological Science*, 38(6): 1308 – 1313.
- 390 Homsy C. A., Tullos H.S., Anderson M. S. (1972), Some physiological aspects of prosthesis
391 stabilization with acrylic polymer. *Clinical Orthopaedics and Related Research*,
392 83:317 – 328.
- 393 Kweon C., McLaren A. C., Leon C., McLeomore R. (2011), Amphotericin B Delivery from
394 bone cement increases with porosity but strength decreases. *Clinical Orthopaedics*
395 *and Related Research*, 469(11): 3002 – 3007.
- 396 Landgraf R., Ihlemann J., Kolmeder S., Lion A., Lebsack H., Kober C. (2015), Modelling
397 and simulation of acrylic bone cement injection and curing within the framework of
398 vertebroplasty. *ZAMM - Zeitschrift für angewandte Mathematik und Mechanik*, 1 –
399 26, DOI 10.1002/zamm.201400064.
- 400 Lewis G. (1997), Properties of acrylic bone cement: state of the art review. *Journal of*
401 *Biomed. Mater. Res. B (Appl. Biomater.)*, 38(2): 155 – 182.
- 402 Maletijt J.D. W., Sloof T.J.J. H., Huiskes R. (1987), The actual status of acrylic bonecement
403 in total hip replacement. *Acta Orthopaedica Belga*, 53: 52 – 58.
- 404 McLaren A. C. (2004), Alternative Materials to Acrylic Bone Cement for Delivery of Depot
405 Antibiotics in Orthopaedic Infections. *Clinical Orthopaedics and Related Research*,
406 427: 101 – 106.
- 407 Mj[^]berg B., Petterson H., Rosenquist R. (1984), Bone cement, thermal injury and the
408 radiolucent zone. *Acta Orthopaedica Scand*, 55:597 – 600.
- 409 MIT (revived 2017), Material Property
410 database.http://www.io.tudelft.nl/research/dfs/idemat/Onl_db/Id123p.htm.
- 411 Noble, P. C. (1983), Selection of acrylic bone cements for use in joint replacement.
412 *Biomaterials*, 4: 94 – 100.
- 413 Pal, S. (2014), Design of Artificial Human Joints and Organs. *Springer-Verlag New York*
414 *Inc.*, 2014 Ed. 1 – 419.
- 415 Peter, S. J., Kim, P., and Yasko, A.W. (1999), Crosslinking characteristics of an
416 injectable poly(propylene fumarate)/ β -tricalcium phosphate paste and mechanical
417 properties of the crosslinked composite for use as a biodegradable bone cement. *J*
418 *Biomed Mater Res.*, 44: 314 – 32.

- 419 Perez M. A., Nuno N., Madrala A., Garcia-Aznar J. M., Doblara M. (2009), Computational
420 Modelling of Bone Cement Polymerization: Temperature and Residual Stresses.
421 *Computers in Biology and Medicine*, 39(9): 751 – 759.
- 422 Rho J. Y., Ashman R. B., Turner C. H. (1993), Young's Modulus of Trabecular and Cortical
423 Bone Material: Ultrasonic and Microensile Measurements. *Journal of Biomech.*,
424 26(2): 111 – 119.
- 425 Swenson Jr. L. W. and Schurman D. J. (1981), Finite element temperature analysis of a total
426 hip replacement and measurement of PMMA curing temperature. *J Biomed Mater*
427 *Res*, 15
- 428 Tang, I – Ming. (2011), Finite element method. *International journal of mechanics*, 5: 204.
- 429 Vaishya R., Chanhani M., Vaish A. (2013). Bone Cement. *Journal of Clinical Orthopadics*
430 *and Trauma*, 4(4): 157 – 163.
- 431 Vaishya R., Vaish A., Nadeem A. (2013), Bisphosphonate Induced atypical subtrochanteric
432 demoral fracture. *BMJ Case Report 2013*, DOI:10.1136/bcr-2013-201931.
- 433 Wapler M. C., Leupold J., Dragonu I., von Elverfeldt D., Zaitsev M., Wallrabe U. (2014),
434 Magnetic properties of materials for MR engineering, micro-MR and beyond. *JMR*,
435 242: 233–242. doi:10.1016/j.jmr.2014.02.005.
- 436 Yamamoto T., Nakamura T., and Iida H. (1998), Development of Bioactive Bone Cement
437 and its Clinical Applications. *Biomaterials*, 19(16):1479 – 1482.